JOURNAL OF SPACECRAFT AND ROCKETS
Vol. 35, No. 1, January–February 1998

Sheath Structure Around a High-Voltage Body in Magnetized Nonflowing Ionospheric Plasma

Mengu Cho*
Kyushu Institute of Technology, Tobata-ku, Kitakyushu 804, Japan

The electron sheath structure around a cylindrical body with a finite length biased to a high positive potential in a magnetized nonflowing plasma in low Earth orbit is studied. The results of Monte Carlo particle-in-cell simulations show that once electrons lose their energy by scattering due to the collective action of plasma, they are trapped by the potential well inside the sheath and enhance the electron density near the body surface parallel to the magnetic field. On the basis of simulation results, the electron density inside the sheath can be approximated by a uniform density. The electron density and potential structure inside the sheath are formulated as functions of magnetic field strength, plasma density, cylinder radius, and body potential. The accuracy of the theoretical formulas is evaluated by comparing the theoretical results with the simulation results.

Nomenclature

B = magnetic field, G
E = electric field, V/m
f, g = periodic functions
I_{eo} = total electron current to upper half of cylindrical body, A
L = axial half length of trapped zone, m
L_c = axial half length of cylindrical body, m
m = particle mass, kg
n = number density, m^{-3}
n_o = electron density of ambient Maxwellian plasma, m^{-3}
q = charge of one superparticle
r_c = collection radius, m
r_i = inner turning point of electron, m
r_L = radial boundary position, m
r_o = outer turning point of electron, m
r_{PM} = Parker–Murphy radius, m
r_p = cylindrical body radius, m
r_s = sheath boundary radius, m
T = temperature, K
v = velocity, m s^{-1}
v_o = electron thermal flux velocity, m s^{-1}
z_L = axial boundary position, m
Γ_{er} = electron radial flux, m^{-2} s^{-1}
Γ_{ez} = electron axial flux, m^{-2} s^{-1}
λ_{de} = electron debye length, m
ν_{es} = effective scattering frequency, s^{-1}
ϕ_p = body surface potential, V
ω_{ce} = electron gyrofrequency, absorbed radiation per second
ω_{pe} = electron plasma frequency, absorbed radiation per second, $\sqrt{(n_o e^2/\epsilon_o m_e)}$

Subscripts

e = electron
i = ion
n = neutral
r = radial direction
z = axial direction

Introduction

THE use of high power in future space missions, especially in low Earth orbit (LEO), calls for high-voltage power generation and transmission, typically higher than 100 V. The operation at high voltage, however, may cause serious environmental interaction between the spacecraft and the ionospheric plasma. A key factor that determines the nature of the spacecraft–plasma interaction is the electric sheath structure around the spacecraft body.

This paper is the first half of a report of the results of theoretical and computational work on the sheath structure around a cylindrical body with a finite length and with a high positive potential in ionospheric nonflowing magnetoplasma conditions. The second half of the report[1] focuses on the effects of ionization on the sheath structure and derivation of a theoretical formula to express the critical neutral density above which the sheath boundary expands infinitely. The work presented in this paper forms the basis of Ref. 1. The purpose of this paper is to conduct theoretical formulation on the electron density and the potential structure inside the sheath at the limit of low neutral density, where the neutral density around the object is equal to the ambient undisturbed values. Reference 1 discusses the case in which neutral density is enhanced for various reasons, such as thruster firing or surface outgassing.

Laframboise and Sonmar[2] made a detailed review of previous theoretical work on the subject of the electron current collection by a biased body in collisionless magnetoplasma. If only the space charge effects are included and the magnetic field is neglected, the theory by Langmuir and Blodgett[3] gives the current collection by a spherical body under the assumption that the particles are accelerated in the radial direction only. Even taking into account the nonradial velocities, as long as the magnetic field is neglected, the collisionless probe theory that integrates the Vlasov equation including the self-consistent space charge has been already established (for example, see Ref. 4).

If the geomagnetic field is included, the theoretical treatment becomes increasingly difficult. The work of Parker and Murphy[5] has been cited by many for the magnetized case. From the conservation of angular momentum and total energy, they gave

$$r_{PM} = r_p \left[1 + \sqrt{\frac{8e\phi_p}{m_e \omega_{ce}^2 r_p^2}} \right]^{\frac{1}{2}} \tag{1}$$

as the upper limit on the radius of particle collection by a spherical body. The radius of particle collection means that the initial radius in a cylindrical coordinate system taking the magnetic field in the axial direction must be within that radius for a particle at infinity to be collected by the body. The electron current calculated by multiplying the electron thermal flux by the cross-sectional area of πr_{PM}^2 has been used in many space experiments as a reference value to study the electron current collection by a spacecraft, including the latest tethered satellite system (TSS) experiments.[6] The current calculated based on Langmuir–Blodgett theory[3] has served as another reference in the experiments. The theory of Parker and Murphy applies to the case in which debye length is much longer

Received March 13, 1997; revision received Sept. 26, 1997; accepted for publication Oct. 14, 1997.

*Associate Professor, Department of Electrical Engineering. E-mail: cho@ele.kyutech.ac.jp. Member AIAA.

than the characteristic length of the body. This paper deals with the case in which the characteristic body scale is much larger than the debye length. The space charge effect inside the sheath is crucial for determining the shape of the sheath; the magnetic field is also important for defining the particle trajectory inside the sheath.

Ma and Schunk[7] studied the sheath structure around a high-voltage sphere by computer simulations with a fluid code. They showed that the electron density is enhanced near the body surface because of $E \times B$ drift, and the results agree qualitatively with the experimental results of Greaves et al.,[8] who showed that a stable toroidal plasma could form around a positively biased spherical electrode in the presence of a low-pressure gas in a uniform magnetic field. However, the fluid code lacks the capability to reproduce the electron diffusion across the magnetic field that results from the kinetic interaction between the plasma and the time-varying electrostatic field. A particle-in-cell (PIC) code can simulate the kinetic interaction by solving the particle motion self-consistently with the time-varying electric field and the space charge density. Usui[9] made a computational study on the sheath structure around a high-voltage object in ionospheric plasma by using a PIC code and found that the electron density inside the sheath was relatively uniform up to $e\phi_p/\kappa T_{eo} \simeq 1000$, even though he simulated the case of a very small object whose characteristic length is only 6 times the debye length.

The largest difference between this work and previous theoretical and computational works is that extensive use is made of a Monte Carlo PIC (MC-PIC) code to check the numerical accuracy of the theoretical formulations. The MC-PIC simulation is used as a numerical experiment to supplement the laboratory experiment that is necessary to check the theory developed here, but it is very difficult to conduct. The MC-PIC code can correctly simulate the kinetic interaction between the plasma particles and the electrostatic waves as well as the collision between the plasma particles and the neutral gas surrounding the object. The collisional transport of electrons across the magnetic field could be important when the neutral gas density is enhanced near the spacecraft body surface.

This paper neglects the orbital velocity of the body, which could be a very important parameter for defining the sheath structure around spacecraft in orbit. Because the orbital velocity is much less than the electron thermal speed, as long as the orbital velocity is parallel to the magnetic field the effects caused by neglecting it should be minimal. To investigate its effect when the orbital velocity has some angle with respect to the magnetic field, a three-dimensional simulation code is needed, which requires far more computational resource than the two-dimensional simulation presented here. Developing a three-dimensional code and studying the combined effects of magnetic field and orbital velocity has been tried by several authors, and preliminary results[10,11] show asymmetry between the ram and wake directions. When the magnetic field is perpendicular to the orbital velocity, asymmetry develops even in the direction perpendicular to both the magnetic field and the orbital velocity, which results from $E \times B$ drift of electrons. The theoretical formula derived in this paper may not be directly applicable to spacecraft flying LEO. The work presented here, however, represents an intermediate step to construct a theory applicable to more realistic situations and still serves as a useful starting point for more difficult work.

The first part of this paper describes the result of particle simulation to study the effect of magnetic field on the electric sheath structure. In the second part of the paper, formulas are derived to calculate the electron density near the side surface of the cylindrical body and the sheath radius around the cylinder body, and assumptions and approximations are made to derive simple formulas to calculate the electron density and the sheath radius even with a calculator to allow study over a wide range of parameters. To evaluate the accuracy of the assumptions and approximations, the MC-PIC simulations are used extensively as numerical experiments.

MC-PIC Simulation

Simulation Code

The MC-PIC code used in this paper is two-dimensional in space and three-dimensional in velocity. An axisymmetric cylindrical coordinate system is used whose axis is the same as the axis of a cylindrical body as shown in Fig. 1. I assume no spatial gradient in the azimuthal direction and I assume symmetry around the axis. I also assume symmetry across the $z = 0$ plane and calculate only the upper half of the cylinder. Electrons and ions are injected from the two boundaries $r = r_L$ and $z = z_L$ with Maxwellian distribution and no drift velocity. When a magnetic field is included in the simulation, the magnetic field is parallel to the z axis. I call the body surface facing the $z = z_L$ boundary the top surface and the surface facing the $r = r_L$ boundary the side surface. These terminologies are indicated in Fig. 1. The boundaries parallel to each surface are called top and side boundaries. The boundary at the central axis is called the center boundary and the boundary at $z = 0$ is called the bottom boundary.

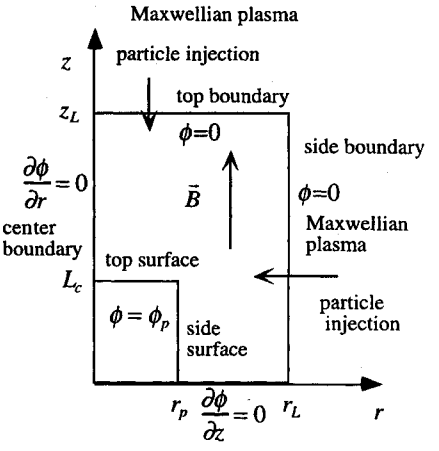

Fig. 1 Schematic picture of simulation space.

In the MC-PIC simulation, the motion of many superparticles is followed, each of which represents a group of real charged particles. Particles that exit the computational domain from the bottom boundary are reinjected with the opposite axial velocity. It is assumed that all of the particles that hit the body surface are absorbed. For the ion-to-electron mass ratio, $m_{ai}/m_e = 10$ is used for the ambient ions that fill the computational domain initially and are injected from the top and side boundaries. The charge of each superparticle for the ambient ions is equal to the absolute value of the electron charge, i.e., $q_{ai} = |q_e|$. To justify the use of low mass ratio m_{ai}/m_e, simulations were carried out with $m_{ai}/m_e = 30{,}000$ and $m_{ai}/m_e = 1000$, whose results showed no significant difference from the results with $m_{ai}/m_e = 10$.

The computational domain is filled with water vapor of uniform density $n_n = 10^{15}\ \mathrm{m}^{-3}$ unless stated otherwise. This value is chosen as a typical value of undisturbed neutral density in LEO. For the neutral density of $n_n = 10^{15}\ \mathrm{m}^{-3}$, the effect due to collisions is negligible. Therefore, the simulation in this paper is almost identical to a mere PIC simulation and the MC-PIC code is used only for consistency with the cases of enhanced neutral density, whose results are presented in detail in Ref. 1. The choice of neutral species, water vapor, also comes from the need for consistency with Ref. 1, where water vapor was chosen because it is the major species of outgassing from the spacecraft surface.

Table 1 lists the parameters used for the MC-PIC simulations and the results. The simulation results and the theoretical results in the table are discussed in the following sections. Initially, the simulation space is filled with electrons and ions of Maxwellian distribution with $\kappa T_{eo}(= 0.2$ or 0.1 eV) and $\kappa T_i = 0.1$ eV and density n_o. The grid sizes are $\Delta z = \Delta r = 0.02$ m for $n_o = 10^{11}\ \mathrm{m}^{-3}$ and $\Delta z = \Delta r = 0.04$ m for $n_o = 10^{10}\ \mathrm{m}^{-3}$, which correspond to $\Delta z/\lambda_{de} \leq 2$. The total number of superparticles that initially fill the simulation space is 10^5–10^6 for each species, depending on the size of simulation space, but is set so that at least 10 particles are placed in one grid cell. If equal charge and mass are assigned to each superparticle, the number of superparticles proportional to the cell volume becomes increasingly small near the central axis. Therefore, the charge and mass of superparticles were adjusted and the q/m ratio was kept constant so that there are as many particles at a small radius as at a larger radius.

Table 1 Parameters of MC-PIC simulation, results of simulation, and results of theory

							Simulation results			Theoretical results			
No.	n_o, m	B, G	r_p, m	L_c, m	ϕ, V	κT_{eo}, eV	$\overline{n_e}/n_o$ [Eq. (21)]	r_c, m	r_s, m	n_e/n_o [Eq. (20)]	r_{PM}, m [Eq. (1)]	r_s, m [Eq. (22)]	n_e/n_o [Eq. (23)]
1	10^{11}	0.35	0.48	0.48	100	0.2	0.26	1.06	1.10	0.14	1.07	1.14	0.18
2	10^{11}	0	0.48	0.48	100	0.2							
3	10^{11}	0.35	0.48	0.48	200	0.2	0.30	1.13	1.27	0.24	1.24	1.35	0.21
4	10^{11}	0.35	0.48	0.96	100	0.2	0.19	0.93	1.09	0.29	1.07	1.14	0.18
5	10^{11}	0.35	0.48	0.96	200	0.2	0.26	1.24	1.29	0.14	1.24	1.35	0.21
6	10^{11}	0.35	0.96	0.48	100	0.2	0.17	1.41	1.66	0.32	1.66	1.72	0.15
7	10^{10}	0.35	0.48	0.96	100	0.1	1.02	0.98	1.32	1.11	1.07	1.35	1.00
8	10^{10}	0.35	0.48	0.96	200	0.1	1.09	1.19	1.64	1.11	1.24	1.64	1.05
9	10^{10}	0.35	0.48	0.96	300	0.1	1.12	1.29	1.84	1.14	1.35	1.85	1.09
10	10^{10}	0.35	0.48	0.96	400	0.1	1.22	1.40	2.08	1.17	1.44	2.03	1.12
11	10^{10}	0.35	0.48	1.92	100	0.1	0.78	0.97	1.44	1.21	1.07	1.35	1.00
12	10^{11}	0.35	0.24	0.48	100	0.2	0.35	0.72	0.77	0.18	0.72	0.80	0.22
13	10^{11}	0.35	0.48	0.48	300	0.2	0.34	1.27	1.39	0.21	1.35	1.49	0.22
14	10^{11}	0.50	0.48	0.48	100	0.2	0.36	0.91	0.99	0.32	0.94	1.01	0.29
15	10^{11}	0.20	0.48	0.48	100	0.2	0.12	1.25	1.40	0.08	1.36	1.42	0.09

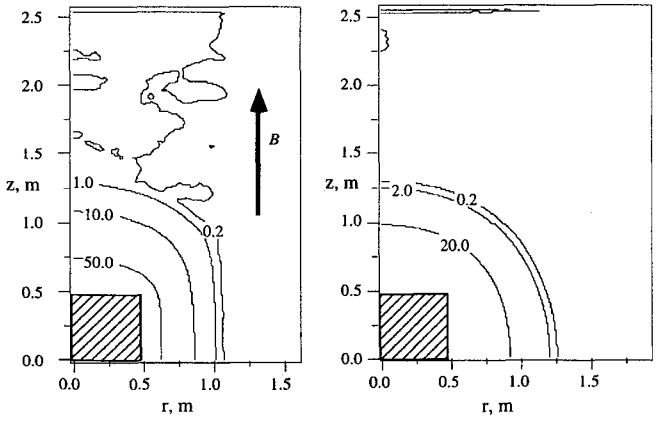

a) With magnetic field [case (1)] **b) Without magnetic field [case (2)]**

Fig. 2 Electric potential around a cylindrical body biased to 100 V.

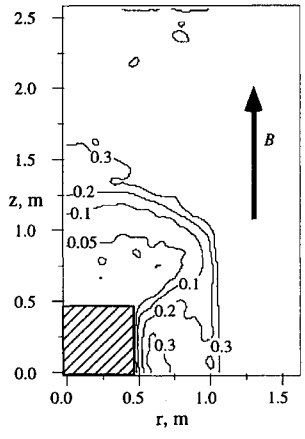

Fig. 3 Electron density around a cylindrical body biased to 100 V with magnetic field [case (1)].

The body potential is suddenly raised to a nonzero value ϕ_p at time $t = 0$ and fixed to this value after $t = 0$. Generally, as the simulation begins by suddenly biasing the object in the uniform Maxwellian plasma, the electric potential of a given point has an initial disturbance of the order of the ion plasma frequency. The amplitude of the initial disturbance decays exponentially and, after it decays, the electric potential remains steady with fluctuation of some amplitude. Typically the MC-PIC code is run up to $t = 300\pi/\omega_{pe}$ with a time step of $\Delta t = 0.02/\omega_{pe}$.

Simulation Results

Figure 2b shows the steady-state electric potential contours for case (2), where there is no magnetic field. The shaded area denotes the cylinder body, and the contour labels are in volts. The sheath structure is almost spherical because the radius of the cylindrical body r_p is the same as its half length L_c, and the sheath is thick enough to hide the geometry of the body. The sheath boundary at the $z = 0$ plane is 1.26 m and the boundary off the edge of the cylinder is 1.33 m. The result of the nonmagnetized case can be checked against the theory of Langmuir and Blodgett[3] by comparing the sheath radius. The Poisson equation is integrated with the initial condition for the particle velocity at the sheath edge, and the sheath radius is determined so that the resulting potential structure satisfies the boundary conditions. More details of the computational procedure are given in Ref. 12. The sheath radius calculated in this way is 1.20 m for a cylinder with a radius of 0.48 m and 1.29 m for a sphere with a radius of 0.67 m. The radius of 0.67 m corresponds to the distance from the center to the end of the cylinder. The results show reasonable agreement, which validates the MC-PIC code.

Figure 2a shows the electric potential contours for case (1), where the magnetic field of 0.35 G parallel to the z axis is included and the sheath thickness is decreased perpendicular to the magnetic field and the thickness along the magnetic field line is unchanged. As the magnetic field is increased, the sheath is suppressed further, which is confirmed by the results of cases (14) and (15). Suppression of the sheath is explained by examining the electron densities around the body. The electron density around the body for case (1) is shown in Fig. 3, where the contour labels are in n_e/n_o. When there is no magnetic field, the electron density decreases radially toward the body surface from the sheath edge. When there is a magnetic field, there is a bump in the electron density at the side of the body. This bump is formed by electrons that are trapped in the potential well by losing their energy via scattering because of collective action of the plasma and by electrons that rotate around the body by $E \times B$ drift.

Figure 4 presents examples of particle trajectories for case (1). To plot Fig. 4, several particles injected from the top boundary between $t = 300\pi/\omega_{pe}$ and $(300\pi + 0.2)/\omega_{pe}$ were tagged and their position at every time step was stored until they exited the simulation space while the MC-PIC code was run for another $300\pi/\omega_{pe}$. To make it easy to understand, the particle trajectories after they crossed the bottom boundary, $z = 0$, were transformed to the trajectories at $z < 0$, by using the mirror image across $z = 0$.

When the electric field is completely stationary, electrons have two constants of motion, namely, the canonical momentum and the total energy, as discussed in Refs. 4 and 5. For a given set of the canonical momentum and the total energy, the boundary of allowed particle positions can be drawn on the $r - z$ plane. They are defined by the innermost and outermost turning points of gyromotion as the electrons move along the magnetic field. These boundaries are the same ones shown as a magnetic bottle in Figs. 1, 4, and 16 of Ref. 2. There are three types of electron motion inside the boundaries. The first type (type 1 in Fig. 4) is made of electrons whose innermost turning points of gyromotion cross the body surface and are collected by the body. The second type (type 2 in Fig. 4) is made of electrons

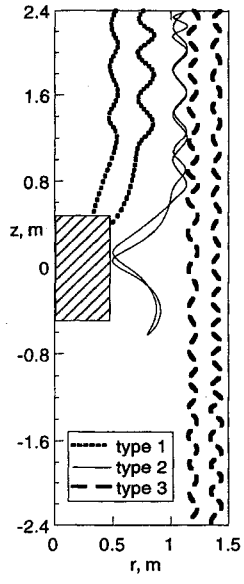

Fig. 4 Example of electron trajectory for case (1) in the MC-PIC simulation.

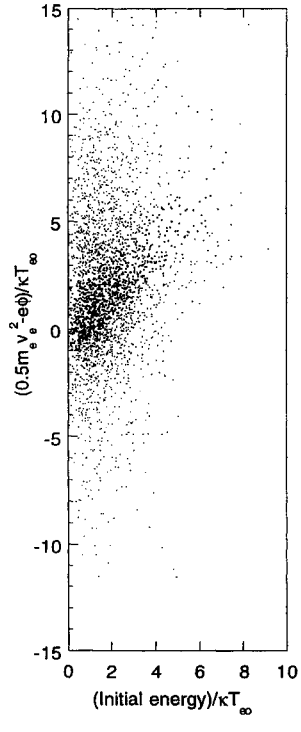

Fig. 5 Initial energy and total energy of electrons within $0 < z < 0.2$ m and $0.48\,\text{m} < r < 1.1$ m at $t = 300\pi/\omega_{pe}$ for case (1) in the MC-PIC simulation.

whose innermost turning points do not cross the body surface but are significantly bent toward the body surface inside the sheath. They go back and forth inside the sheath and finally escape the sheath while keeping their initial energy and canonical momentum. The third type of electron (type 3 in Fig. 4) is those not affected by the presence of the body, whose innermost and outermost boundaries are just parallel lines along the magnetic field line. The type of an electron is determined by the initial position r and the initial velocities at the top boundary.

When the electric field is not stationary and varies in time, there are two additional types of electron motion. As the space charge density fluctuates via collective action of the plasma, electrostatic waves are excited. Some electrons lose their energy to the wave if their velocities are slightly faster than the wave phase velocity, and some gain energy if the velocities are slightly slower, as it is often explained as a mechanism of Landau damping (see Ref. 13 for an example). The energy loss mechanism is equivalent to scattering of electrons due to collective action of the plasma. I call those electrons that lose energy type 4 electrons, and those that gain energy are type 5 electrons. Once the energy changes from the initial value, a fixed boundary of allowed positions in the $r-z$ plane can no longer be defined. Figure 5 plots the total energy, $\frac{1}{2}m_e v_e^2 - e\phi$, against

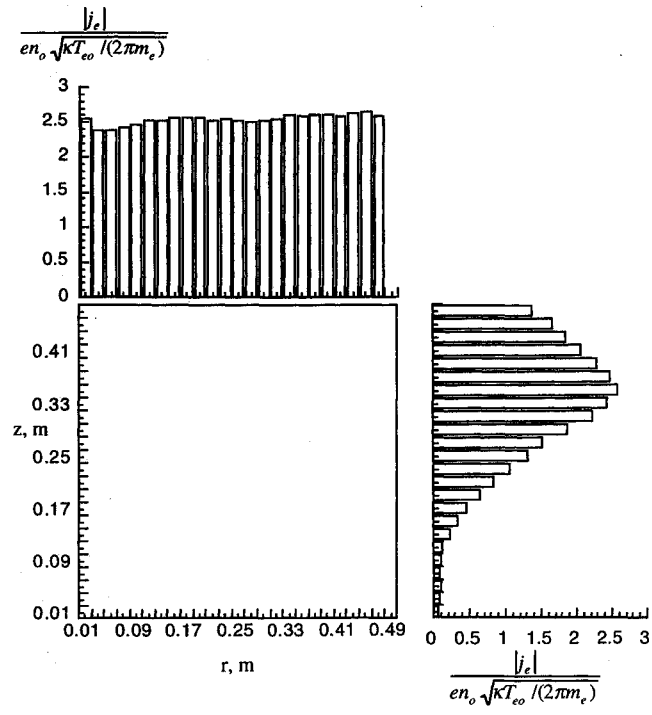

Fig. 6 Current density to each grid cell on the body surface for case (1) in the MC-PIC simulation.

the initial energy for each particle at $0.48\,\text{m} < r < 1.10\,\text{m}$ and $0 < z < 0.2$ m for case (1) at $t = 300\pi/\omega_{pe}$. The energies are normalized by the temperature κT_{eo}. When particles are injected from the top or side boundaries, where $\phi = 0$, they have an initial energy determined by the Maxwellian distribution with the temperature of T_{eo}. A significant number of particles lose their initial energy and have negative energies. Many particles also gain energy. Electron heating was observed during the first TSS flight and offers an explanation for the additional current to the TSS subsatellite anode found in TSS-1R.[14]

The type 5 electrons are heated and the width of the magnetic bottle becomes larger. They either are collected by the body surface like the type 1 electrons or exit the sheath like the type 2 electrons. The type 4 electrons lose energy and can no longer escape the sheath in the axial direction because they cannot overcome the potential well. Their magnetic bottle shrinks compared with the initial shape and the open ends in the axial direction that existed initially are now closed, which means they are trapped. They are removed from the sheath only by being collected by the body surface across the magnetic field or heated to have enough energy to escape the sheath in the axial direction. Either way, they stay inside the sheath for a long time and contribute significantly to the space charge. When the effect of collisions is as significant as the collective action of the plasma in causing an electron to lose its energy, type 4 electrons are also created by collisions.

Figure 6 shows the current density to each grid cell on the cylinder surface for case (1), as the time average between $t = 280\pi/\omega_{pe}$ and $300\pi/\omega_{pe}$. The current density is normalized by the electron thermal current $en_o v_o$, where v_o is defined by

$$v_o = \sqrt{\kappa T_{eo}/2\pi m_e} \tag{2}$$

If we calculate the total current to the upper half body of the cylinder by integrating the current density, we have $|I_{eo}| = 4.84 n_o v_o \pi r_p^2$. I define a hypothetical cylinder as follows: if a particle has its initial position inside the cylinder at $z \to \infty$, it is collected. Such a radius of the hypothetical cylindrical cross section is defined by

$$r_c' = \sqrt{\frac{|I_{eo}|}{en_o v_o \pi}} \tag{3}$$

This radius, r_c' is $\sqrt{(4.84)}\, r_p = 1.06$ m for case (1). In Fig. 2, the contour of $e\phi = \kappa T_{eo} = 0.2$ eV is at 1.10 m at $z = 0$. Therefore,

not all of the electrons entering the sheath are collected by the body. Some of the electrons rotate around the body because of the $E \times B$ drift and escape in the z direction as type 2 or 5 electrons.

Figure 6 shows that a nonzero current flows even to the side surface near $z = 0$. Also the current density to this part of the cylinder is relatively uniform at $|j_e| = 0.09 e n_o v_o$. The current to the side surface near $z = L_c$ is due to electrons whose gyromotions have their inner turning point at $r < r_p$ (type 1 electrons). The current to the side surface near $z = 0$ cannot be explained by this mechanism, and it should be attributed to transport across the magnetic field by type 4 and 5 electrons. The current due to type 1 electrons dominates the current due to type 4 and 5 electrons for a cylinder of modest length.

Theoretical Formulation

Continuity Equation for Trapped Electron

I consider a way to express the electron density near the body side surface. I define a volume of trapped zone next to the side surface, which is shown in Fig. 7, where the definition of L is somewhat ambiguous. It is not the cylinder half length L_c. It should be regarded as the point where the electron current to the side surface becomes very low and uniform and the cross field flux due to type 4 and 5 electrons becomes dominant over the flux of type 1 electrons. For the case shown in Fig. 6 [case (1)], the value of L is approximately $L \simeq 0.1$ m. Later we find that the parameter L is canceled when we calculate the electron density.

I consider the continuity equation for the trapped (type 4) electrons in the volume. At steady state, it is written as

$$\frac{1}{r}\frac{\partial}{\partial r}(n_{e4} v_{er} r) + \frac{\partial}{\partial z}(n_{e4} v_{ez}) = 0 \tag{4}$$

I integrate Eq. (4) in the volume $-L \le z \le L$ and $r_p \le r \le r_s$ and obtain

$$\int_{-L}^{L} \Gamma_{er}|_{r=r_s} r_s \, dz - \int_{-L}^{L} \Gamma_{er}|_{r=r_p} r_p \, dz + 2\int_{r_p}^{r_s} \Gamma_{ez}|_{z=L} r \, dr = 0 \tag{5}$$

where the factor 2 in front of the third term comes from the fact that

$$\int_{r_p}^{r_s} \Gamma_{ez}|_{z=L} r \, dr \quad \text{and} \quad -\int_{r_p}^{r_s} \Gamma_{ez}|_{z=-L} r \, dr$$

where $\Gamma_{ez} = n_{e4} v_{ez}$, are equal because of symmetry across the $z = 0$ plane.

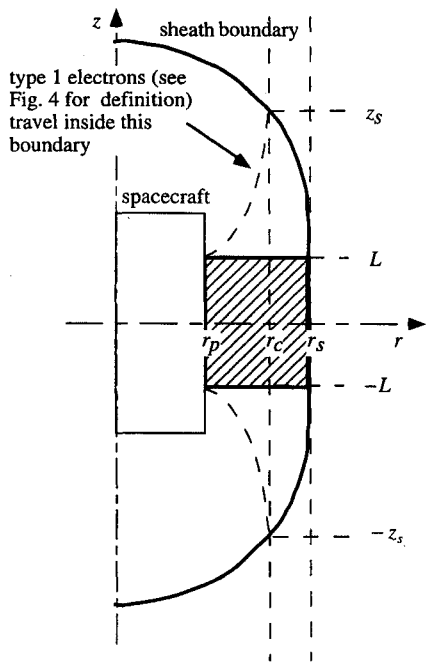

Fig. 7 Volume of trapped zone.

An electron enters the sheath if its radial position at $z = z_s$ is within the radius r_s. But an electron whose radial position at $z = z_s$ is within the radius r_c is collected directly by the body before it reaches $z = L$. I call this radius r_c the collection radius in this paper. Therefore, the total number of electrons that enter the volume from $z = L$ per unit time is given by

$$n_o v_o \pi \frac{r_s^2 - r_c^2}{2} \tag{6}$$

The ratio of the number of trapped electrons to the number of electrons given by Eq. (6) is the probability P that an electron is trapped while it travels from $z = z_s$ to $-z_s$. Once it loses energy by scattering due to collective action of the plasma, it is trapped in the potential well and cannot escape in the axial direction. I denote the time scale on which electrons lose their energy by $1/\nu_{es}$. I assume that the trapped electrons are transported only radially toward the body side surface across the magnetic field and escape the volume only by being collected at the body surface. Therefore, at steady state,

$$\int_{r_p}^{r_s} \Gamma_{ez}|_{z=L} r \, dr = -P n_o v_o \pi \frac{r_s^2 - r_c^2}{2} \tag{7}$$

and the probability P is given by

$$P = 1 - \exp\left(-\int_{z_s}^{-z_s} \frac{\nu_{es}}{v_{ez}} dz\right) \tag{8}$$

When

$$\int_{z_s}^{-z_s} \frac{\nu_{es}}{v_{ez}} dz$$

is much smaller than unity, we can expand the exponential of Eq. (8). We also approximate the integral

$$\int_{z_s}^{-z_s} \frac{\nu_{es}}{v_s} dz$$

as follows:

$$\int_{z_s}^{-z_s} \frac{\nu_{es}}{v_{ez}} dz \simeq \frac{2L}{v_o} \nu_{es} \tag{9}$$

Then, Eq. (5) gives

$$\int_{-L}^{L} \Gamma_{er}|_{r=r_s} r_s \, dz - \int_{-L}^{L} \Gamma_{er}|_{r=r_p} r_p \, dz - 2L n_o \nu_{es}\left(r_s^2 - r_c^2\right) = 0 \tag{10}$$

Strictly speaking, equating

$$-P n_o v_o \pi \left\{\frac{r_s^2 - r_c^2}{2}\right\} \quad \text{to} \quad \int_{r_p}^{r_s} \Gamma_{ez}|_{z=L} r \, dr$$

ignores the electrons collected by the body surface at $z > L$ and $z < -L$. It also ignores the electrons that escape axially by gaining energy again through the interaction with waves. The error associated to this equation is further discussed in the next section.

Poisson Equation

I define the sheath boundary as the point beyond which the charge neutrality no longer holds and the electron density is higher than the ambient ion density. The charge neutrality holds in the presheath although the plasma density decreases toward the body surface. In this analysis, I consider only the region between the body surface and the sheath boundary. The potential increases gradually from zero at the edge of the presheath to a potential of the order of the plasma temperature ($0.1 \sim 0.2$ eV) at the sheath boundary. The boundary conditions imposed at the sheath boundary $r = r_s$ are

$$\phi|_{r=r_s} = 0 \tag{11}$$

$$\left.\frac{\partial \phi}{\partial r}\right|_{r=r_s} = 0 \tag{12}$$

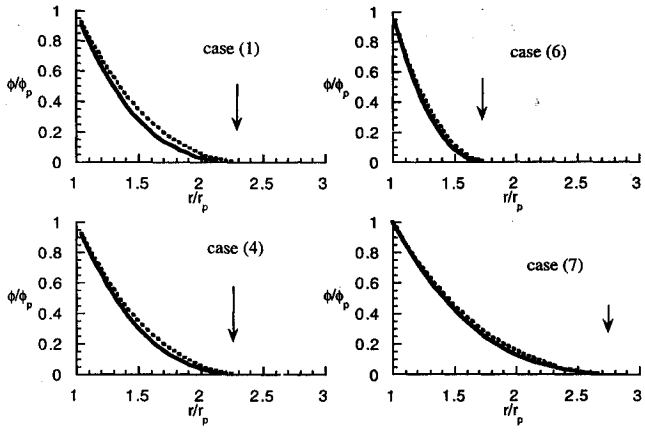

Fig. 8 Electric potential distribution at $z = 0$ for various cases in Table 1: ——, MC-PIC simulation and - - - -, theoretical results from Eqs. (16) and (22).

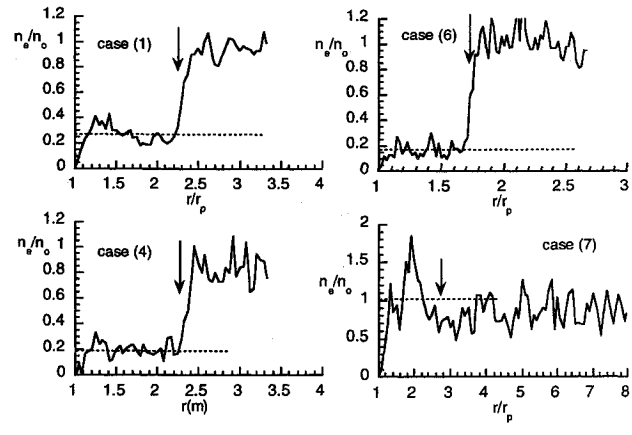

Fig. 9 Electron density distribution at $z = 0$ for various cases calculated by the MC-PIC code.

At the body surface $r = r_p$, I impose

$$\phi|_{r=r_p} = \phi_p \tag{13}$$

The use of Eq. (11) is justified because the potential at the sheath boundary, which is of the order of plasma temperature, can be neglected compared with the surface potential ϕ_p. The electric field should have a nonzero value at the sheath boundary, but it is very weak compared with the surface field or the average electric field inside the sheath. In Fig. 8 the electric potential distribution at $z = 0$ is plotted for various cases listed in Table 1. The solid curves denote the MC-PIC simulation results, and arrows indicate the position of sheath boundary r_s. The sheath boundary is defined as the point where the charge density first becomes zero as we move away from the body surface r_p. The field decreases rapidly near r_s and becomes negligible compared with the field inside the sheath. Therefore, the electric field at the sheath boundary is neglected.

The sheath boundary is determined by the amount of negative charge inside the sheath to shield the effect of positive potential of the body. The Poisson equation in cylindrical coordinates with azimuthal symmetry is written as

$$\frac{1}{r}\frac{\partial}{\partial r}\left(r\frac{\partial\phi}{\partial r}\right) + \frac{\partial}{\partial z}\left(\frac{\partial\phi}{\partial z}\right) = \frac{e}{\epsilon_o}n_e \tag{14}$$

In Eq. (14), the effect of ambient ion density, which is much smaller than the electron density inside the sheath boundary $r < r_s$, is neglected.

Before I proceed with further analysis, I list the major assumptions used in this paper. These assumptions are made only for the parameters inside the volume defined in Fig. 7: Assumption (1), all of the parameters are uniform in the z direction inside the volume; Assumption (2), the electron density between r_p and r_s is uniform; Assumption (3), the effective scattering frequency ν_{es} is uniform in the volume and much less than the electron gyrofrequency ω_{ce}; Assumption (4), the electric field and the potential at the sheath boundary $r = r_s$ are zero; and Assumption (5), the electron density is equal to the density of type 4 electrons.

Assumption (1) is justified by looking at the results of MC-PIC simulations, as in Figs. 2 and 3. To justify the use of Assumption (2), in Fig. 9, I show the electron density along the $z = 0$ line calculated by the MC-PIC code for various cases listed in Table 1. Figure 9 also shows an arrow to indicate the sheath boundary $r = r_s$. The use of Assumption (5) leads to an underestimate of n_e, as there are as many type 2 or 5 electrons as type 4 electrons in Fig. 5. The error associated with this assumption is further discussed in the next section.

From Assumption (1), the second term in Eq. (14) can be neglected. I integrate the Poisson equation from position r inside the sheath to the sheath boundary r_s. Using Assumptions (2) and (4),

$$\frac{\partial\phi}{\partial r} = \frac{e}{\epsilon_o}n_e\left(\frac{r}{2} - \frac{r_s^2}{2}\frac{1}{r}\right) \tag{15}$$

Integrating this further, I obtain

$$\phi(r) = \phi_p\left\{\frac{r_s^2\,\ell n(r_s/r) - \left[\left(r_s^2 - r^2\right)/2\right]}{r_s^2\,\ell n(r_s/r_p) - \left[\left(r_s^2 - r_p^2\right)/2\right]}\right\} \tag{16}$$

Substituting the partial derivative of Eq. (16) with respect to r_s into Eq. (15), I obtain the following relation among n_e, ϕ_p, r_s, and r_p:

$$\phi_p = \frac{e}{\epsilon_o}\frac{n_e}{2}\left[r_s^2\,\ell n\left(\frac{r_s}{r_p}\right) - \frac{r_s^2 - r_p^2}{2}\right] \tag{17}$$

Linson[15] made a similar analysis by using Assumptions (1), (2), and (4) and reached the same equation as Eq. (17). But Linson's theoretical formulation stopped at Eq. (17) and varied the electron density n_e as a parameter. In this present paper, I derive a formula to give n_e and derive an implicit formula to define r_s as a function of ϕ_p without assuming the electron density a priori.

Derivation of Electron Density

The type 4 electrons are transported across the magnetic field by losing their energy on a time scale of $1/\nu_{es}$ while rotating around the magnetic field. Then the radial drift velocity is given by

$$v_{er} = -(e/m_e)E_r\left(\nu_{es}/\omega_{ce}^2\right) \tag{18}$$

The derivation of Eq. (18) is given in the Appendix. The effective scattering frequency ν_{es} due to collective action of the plasma should be comparable with the growth rate of the plasma instability occurring in the trapped zone. Calculating the growth rate and ν_{es} is a very difficult task and is left for future work. If the electron current to the side surface near $z = 0$ shown in Fig. 6 is carried completely by type 4 electrons, which gives an upper limit on ν_{es}, the effective scattering frequency is of the order of $0.01\omega_{pe}$, which is smaller than the gyrofrequency by 2 orders of magnitude. On the basis of this result, I assume that the effective scattering frequency ν_{es} is much less than ω_{ce}.

From Assumption (4) the electron radial flux at r_s, $\Gamma_{er}|_{r=r_s}$, can be neglected compared with $\Gamma_{er}|_{r=r_p}$. Then, Eq. (10) is written as

$$n_{e4}(e/m_e)E_r|_{r=r_p}\left(\nu_{es}/\omega_{ce}^2\right)2Lr_p - 2Ln_o\nu_{es}\left(r_s^2 - r_c^2\right) = 0 \tag{19}$$

where Eq. (18) has been substituted as v_{er} and Assumptions (1) and (2) are used to take out the integral with respect to z. I substitute E_r calculated by Eq. (15) with $r = r_p$ into Eq. (19) and use Assumption (5) to set $n_{e4} = n_e$. Then, finally I obtain

$$n_e = \sqrt{2}n_o\frac{\omega_{ce}}{\omega_{pe}}\sqrt{\frac{r_s^2 - r_c^2}{r_s^2 - r_p^2}} \tag{20}$$

Equation (20) indicates that the electron density does not depend on ν_{es}. Physically, it means that even if the probability of trapping increases, the trapped electrons are transported more easily across

the magnetic field because of higher v_{es}, and the effects cancel each other. I derive the electron density on the assumption that the electrons are trapped by losing their energy by scattering due to collective action of the plasma. The trapping also occurs when electrons lose energy via electron-neutral collisions. For that case, I add the collision frequency to the effective scattering frequency and the derivation thereafter is the same. The resulting equation (20) does not depend on v_{es}, which means that the electron density does not depend on the neutral density as long as the collision frequency is less than the gyrofrequency, which was a basic assumption to obtain Eq. (18).

I now evaluate the accuracy of Eq. (20) by comparing the results with the average electron densities at $z = 0$ obtained from the MC-PIC simulations. I define the average electron density as

$$\overline{n_e} \equiv \left(\int_{r_p}^{r_s} n_e r \, dr\right) \Big/ \left(\frac{r_s^2 - r_p^2}{2}\right) \tag{21}$$

Column 8 of Table 1 lists $\overline{n_e}$. To evaluate Eq. (20), I substitute the values r_s and r_c obtained from the MC-PIC simulations. I approximate r_c by r_c' defined by Eq. (3), where $|I_{eo}|$ is given from the MC-PIC results. This approximation is justified on the basis that the current due to type 1 electrons dominates the current due to type 4 and 5 electrons for a cylinder of modest length. Column 9 of Table 1 gives r_c calculated in this way and column 10 gives r_s taken from the MC-PIC simulation results. Column 11 lists n_e calculated by Eq. (20) with these r_c and r_c. In Fig. 9, I also show the value of column 11 as broken lines. Results of Eq. (20) agree with the average electron density within a factor of 2 for all the cases calculated in this paper.

Discussion

For a long cylinder length L_c, Eq. (20) tends to overestimate the electron density at low ϕ_p [cases (4), (7), (8), and (11)]. There are two reasons for this overestimation. One is that the sheath axial length increases and the assumption $\int v_{es}/v_z \, dt \ll 1$ is no longer true; expanding the exponential in Eq. (8) leads to overestimation of the probability P and the resulting electron density. The other reason is that the approximation given by Eq. (9) gives the overestimation because the axial velocity inside the sheath is faster than v_o due to axial acceleration. At high ϕ_p [cases (5) and (10)] and long L_c, the radial flux Γ_{er} increases because the radial electric field increases. Then approximating r_c by r_c' leads to overestimation of r_c because the current $|I_{eo}|$ in Eq. (3) contains the contribution due to Γ_{er}. This is especially true for a long L_c, such as cases (5) and (10), and leads to an underestimation of n_e.

For a short cylinder length, L_c, [cases (1), (3), (12), (13), (14), and (15)], Eq. (20) tends to underestimate the electron density. For a short cylinder, the use of Eq. (9) underestimates the probability of trapping because the axial path length inside the sheath is longer than the axial length of the volume $2L$. Instead, it should be at least $2z_s$. The effects of using $2L$ and v_o in Eq. (9) somewhat cancel each other and the overall error caused by use of Eq. (9) leads to an estimate within a factor of 2 for short cylinders with $L_c \simeq r_p$.

The other reason for the underestimation for short cylinders is that the contribution of type 2 and 5 electrons to the electron density inside the sheath is neglected. The type 2 electron contribution could become large for a high value of v_{es} where the trapped electrons are quickly transported across the magnetic field, whereas the type 2 electrons move back and forth before they escape the sheath. But high v_{es} means a high probability of trapping for the type 2 electrons. Then the type 2 electrons could become the trapped electrons at any time for a high v_{es}. If the electrons in the volume defined in Fig. 7 are composed of type 2, 4, and 5 electrons with an equal fraction (see Fig. 5), the density n_{e4} in Eq. (19) is replaced by $n_e/3$ and the factor $\sqrt{2}$ in Eq. (20) is replaced by $\sqrt{6}$. The overall estimate obtained from Assumption (5) is within a factor of $\sqrt{3}$.

Derivation of Sheath Boundary Radius

I now make a final assumption to obtain the relationship among ϕ_p, r_s, and r_p. The radius r_c must be a function of n_o, r_p, ϕ_p, T_{eo}, and B. The radius r_{PM} given by Eq. (1) gives an upper limit on r_c for the case of a spherical body and stationary electric field and the following is assumed.

Assumption (6), the radius r_c is approximated by r_{PM}.

In column 12 of Table 1, I list the Parker–Murphy radius r_{PM} for each case. Note that r_{PM} is larger than r_c for all of the cases.

Substituting Eq. (20) into Eq. (17) with r_{PM} as r_c,

$$\phi_p = \frac{e}{\epsilon_o}\frac{n_o}{\sqrt{2}}\frac{\omega_{ce}}{\omega_{pe}} r_p^2 \sqrt{\frac{(r_s/r_p)^2 - 1 - \sqrt{\left(8e\phi_p/m_e\omega_{ce}^2 r_p^2\right)}}{(r_s/r_p)^2 - 1}} \times \left[(r_s/r_p)^2 \ell_n\left(\frac{r_s}{r_p}\right) - \frac{(r_s/r_p)^2 - 1}{2}\right] \tag{22}$$

This equation implicitly gives the sheath radius r_s for a given set of parameters, although a numerical iteration scheme is needed, which is still much cheaper in CPU time than the MC-PIC simulations. Also with Assumption (6), the electron density in the sheath can be calculated by

$$n_e = \sqrt{2} n_o \frac{\omega_{ce}}{\omega_{pe}} \sqrt{\frac{(r_s/r_p)^2 - 1 - \sqrt{\left(8e\phi_p/m_e\omega_{ce}^2 r_p^2\right)}}{(r_s/r_p)^2 - 1}} \tag{23}$$

where r_s can be given as the solution of Eq. (22). Hence, MC-PIC simulations are not needed to calculate the electron density near the side surface.

In columns 13 and 14 of Table 1, I list r_s and n_e, calculated by Eqs. (22) and (23). The sheath radius calculated by Eq. (22) gives a good approximation with a maximum difference of 7% with the MC-PIC simulations results. Generally Eq. (22) gives an overestimate of the sheath radius r_s. The overestimation results from approximating the collection radius r_c by r_{PM}, which is the upper limit on r_c. The overestimate on r_c leads to an overestimate of r_s, which is given as the solution of Eq. (22). The electron density calculated by Eq. (23) still agrees with the average electron density of the MC-PIC simulation results within a factor of 2.

In Fig. 8, I plot $\phi(r)$ given by Eq. (16) with r_s given from the solution of Eq. (22). The analytical formula is plotted as broken curves; solid curves are the MC-PIC results. Agreement between the simulation and theory is very good for cases (4), (6), and (7). It reflects the agreement of the electron densities between the simulation and theory, which are given as columns 8 and 14 of Table 1, respectively. For the other cases, the potential $\phi(r)$ calculated by Eq. (16) overestimates the potential at a given point, because the uniform electron density, which is the basis of Eq. (16), is less than the simulation values. The maximum difference between the two potentials is $0.11\phi_p$ for case (13). The radial electric field at the body surface can be calculated by substituting $r = r_p$ into Eq. (15) along with r_s and n_e determined from Eqs. (22) and (23). Generally, this leads to underestimation of the surface electric field. The maximum error is 21% for case (13).

Conclusion

I have studied the electron sheath structure around a cylindrical body with a finite length biased to a high positive potential in a nonflowing magnetized ionospheric plasma. MC-PIC simulations are used as numerical experiments to check the validity of the theoretical treatment. The results of MC-PIC simulations show that the electrons are trapped by the potential well by losing their energy by scattering due to collective action of the plasma and form a bump in the electron density near the body surface. The results of MC-PIC simulations also show that the electron density near the side surface is relatively uniform.

On the basis of this observation, a theoretical formulation has been tried to describe the electron density and the potential structure as a function of parameters, which are given externally. In other words, I have tried to obtain simple formulas that can calculate the electron density and the potential structure even with a calculator and without the use of expensive MC-PIC simulations.

By defining the probability of trapping with an effective scattering frequency, the number of electrons trapped per unit time can

be defined. The electron velocity across the magnetic field is given once the scattering frequency can be defined. By equating the electron flux of trapped electrons and the electron flux transported to the body side surface, the trapped electron density can be calculated. The trapped electron density obtained in this way is a function of the magnetic field strength, the ambient plasma density, the sheath radius, the cylinder radius, and the electron collection radius. The electron collection radius is the radius of a hypothetical cylindrical cross section, which defines the outer boundary of electrons collected directly by the body surface. With the Parker–Murphy radius used as an approximation on the electron collection radius, an implicit relation among the sheath radius, the magnetic field strength, the ambient electron density, the cylinder radius, and the body potential can be obtained. Therefore, the electron density becomes a function of the magnetic field strength, the ambient plasma density, the cylinder radius, and the body potential only. The electron density calculated by this formula agrees with the results of MC-PIC simulations within a factor of 2.

By using the assumption of uniform electron density inside the sheath, it is easy to integrate the Poisson equation with appropriate boundary conditions. By using the implicit relation between the sheath radius and the other parameters, the potential structure inside the sheath can be calculated as a function of the magnetic field strength, the ambient plasma density, the cylinder radius, and the body potential only. The radius of the sheath boundary is also calculated from the implicit relation and the theoretical results agree with the results of MC-PIC simulations with a maximum error of 7% for the radius of sheath boundary and of 21% for the strength of surface electric field.

Appendix: Derivation of Equation 18

Plamadesso and Ganguli[16] solved the equation of motion of an electron in a cylindrical coordinate system, where the electric field direction is radial only and the magnetic field direction is axial only. When an electron has negligible kinetic energy at $r = r_o$, its radial position has the inner turning point at $r = r_i$. The radial position of the electron oscillates around a mean value $\bar{r} = (r_o + r_i)/2$ with a certain period. It is written as

$$r(t) = \bar{r} + (\delta r/2) f(t) \tag{A1}$$

where $\delta r = r_o - r_i$ and $f(t)$ is a periodic function with an amplitude of unity and a period of τ_c, i.e., $f(t + \tau_c) = f(t)$, and Plamadesso and Ganguli[16] calculated δr as

$$\delta r = -\frac{2e}{m_e \omega_{ce}^2} \frac{\partial \phi}{\partial r}\bigg|_{r=\bar{r}} \tag{A2}$$

When an electron loses its energy as a result of scattering either because of collective action of the plasma or because of collision at $t = t_c$ and $r = r'_o$, its radial position after the scattering is given by

$$r'(t) = \bar{r}' + (\delta r/2) g(t) \tag{A3}$$

where $g(t)$ is another periodic function and it is assumed that the radial electric field is constant between $\bar{r}$ and $\bar{r}'$ and δr does not change. Because after the scattering the electron has the outer turning point at $r = r'_o$, it is possible to write

$$r'(t_c) = r'_o = \bar{r}' + (\delta r/2) \tag{A4}$$

The position r'_o is also given from Eq. (A1) as

$$r'_o = \bar{r} + (\delta r/2) f(t_c) \tag{A5}$$

The shift of average position due to scattering is given by

$$\delta \bar{r} = \bar{r}' - \bar{r} = r'_o - (\delta r/2) - \bar{r} = -(\delta r/2) + (r'_o - \bar{r})$$

$$= -(\delta r/2) + (\delta r/2) f(t_c) \tag{A6}$$

If the timescale of scattering ν_{es}^{-1} is much less than the period τ_c, which is comparable to $2\pi/\omega_{ce}$, it can be assumed that the scattering occurs during $t = t'$ to $t' + \mathrm{d}t'$ with an equal probability of $\nu_{es}\,\mathrm{d}t'$. Then the expected value of $\delta \bar{r}$ after one period of rotation can be calculated as

$$\langle \delta \bar{r} \rangle = \int_0^{\tau_c} \delta \bar{r}(t'_c) \nu_{es}\,\mathrm{d}t'_c = -\nu_{es} \frac{\delta r}{2} \tau_c \left[1 - \frac{1}{\tau_c} \int_o^{\tau_c} f(t'_c)\,\mathrm{d}t'_c \right] \tag{A7}$$

The function $f(t)$ is negative during a half period where $r < \bar{r}$ and positive during the half where $r > \bar{r}$. The time integral of $f(t)$ from 0 to τ_c is not necessarily zero, because an electron can stay longer at $r < \bar{r}$ or $r > \bar{r}$ while rotating around the average position $\bar{r}$. But it certainly should be much less than τ_c and in the bracketed right-hand side of Eq. (A7), the second term is neglected. The radial drift velocity for electrons is given by dividing $\langle \delta \bar{r} \rangle$ by the period τ_c;

$$v_{er} = -\nu_{es} \frac{\delta r}{2} = \frac{2e\nu_{es}}{m_e \omega_{ce}^2} \frac{\partial \phi}{\partial r} \tag{A8}$$

where Eq. (A2) has been substituted for δr.

References

[1]Cho, M., "Ionization Around a High-Voltage Body in Magnetized Nonflowing Ionospheric Plasma," *Journal of Spacecraft and Rockets*, Vol. 35, No. 1, 1998, pp. 90–99.

[2]Laframboise, J. G., and Sonmar, L. J., "Current Collection by Probes and Electrodes in Space Magnetoplasmas: A Review," *Journal of Geophysical Research*, Vol. 98, No. A1, 1993, pp. 337–357.

[3]Langmuir, I., and Blodgett, K. B., "Currents Limited by Space Charge Between Concentric Spheres," *Physics Review*, Vol. 22, No. 1, 1923, pp. 49–59.

[4]Laframboise, J. G., "Theory of Spherical and Cylindrical Langmuir Probes in a Collisionless, Maxwellian Plasma at Rest," Univ. of Toronto, TR UTIAS 100, June 1966.

[5]Parker, L. W., and Murphy, B. L., "Potential Buildup on an Electron-Emitting Ionospheric Satellite," *Journal of Geophysical Research*, Vol. 72, No. 5, 1967, pp. 1631–1636.

[6]Chang, C. L., Droboto, A. T., and Papadopoulos, K., "I-V Characteristics of the Tethered Satellite System," AIAA Paper 97-0584, Jan. 1997.

[7]Ma, T. Z., and Schunk, R. W., "A Fluid Model of High Voltage Spheres in the Ionosphere," *Planetary Space Science*, Vol. 37, No. 1, 1989, pp. 21–47.

[8]Greaves, R. G., Boyd, D. A., Antoniades, J. A., and Ellis, R. F., "Steady-State Toroidal Plasma Around a Spherical Anode in a Magnetic Field," *Physics Review Letters*, Vol. 64, No. 8, 1990, pp. 886–889.

[9]Usui, H., "Study on the Electrodynamic Interaction Between a Tethered Satellite System and Space Plasma," Ph.D. Thesis, Dept. of Electrical Engineering, Kyoto Univ., Kyoto, Japan, Dec. 1993.

[10]Cho, M., "Three-Dimensional Monte Carlo Paricle-in-Cell Simulation of Plasma Environment Around Spacecraft," *Proceedings of KDK Simulation Symposium* (Radio Atmospheric Science Center, Kyoto Univ.), 1996, pp. 59–62.

[11]Chan, C. B., and Singh, N., "3-D Numerical Simulation of the Tethered Satellite: 2. Sheath Structure and Electron and Ion Flow Patterns," American Geophysical Union Fall Meeting, San Francisco, Dec. 1996.

[12]Cho, M., "Ionosphere Ionization Effects on Sheath Structure Around a High-Voltage Spacecraft," *Journal of Spacecraft and Rockets*, Vol. 32, No. 6, 1995, pp. 1018–1026.

[13]Chen, F. F., *Introduction to Plasma Physics and Controlled Fusion*, 2nd ed., Vol. 1, Plenum, New York, 1984, Chap. 7.

[14]Cooke, D., "TSS-IR Electron Currents: Magnetic Limited Collection from Heated Presheath," American Geophysical Union Fall Meeting, San Francisco, Dec. 1996.

[15]Linson, L. M., "Current-Voltage Characteristics of an Electron-Emissing Satellite in the Ionosphere," *Journal of Geophysical Research*, Vol. 74, No. 9, 1969, pp. 2368–2375.

[16]Palmadesso, P. J., and Ganguli, G., "Effects of Plasma Turbulence on Electron Collection by a High-Voltage Spherical Probe in a Magnetized Plasma," *Journal of Geophysical Research*, Vol. 97, No. A5, 1992, pp. 6493–6504.

R. G. Wilmoth
Associate Editor